Influence of Water Condensation on Charge Transport and Electric Breakdown Between an Atomic Force Microscope Tip, Polymeric, and (Semiconductor) CdS Surfaces

Ewa Rowicka, Dmytro Kashyn, Michael A. Reagan, Tadashi Hirano, Pavel B. Paramonov, Ivan Dolog, Robert R. Mallik and Sergei F. Lyuksyutov*

Department of Physics, The University of Akron, Akron OH 44325, USA

Abstract: Water condensation is shown to have a major influence on electric charge transport and nanostructure formation in polymer-, and semiconductor-thin-film surfaces in the proximity of a biased Atomic Force Microscope (AFM) tip. The water forms a meniscus bridge between the AFM tip and the surface to form a three-component system comprised of the AFM tip, water meniscus, and the surface. The associated electric field in the meniscus is spatially non-uniform and has a magnitude of the order of 10^8-10^{10} Vm^{-1}. An intensive experimental analysis of the input and output electric currents in the AFM tip/water meniscus/surface system, performed at various relative humidity levels between 10 and 60%, indicates that the magnitude of the output current, drained from surface, reaches values as large as several μA which exceeds the input current, injected via the AFM tip (0.01-10 nA), by at least an order of magnitude. This effect is particularly evident when the relative humidity is greater than 20-25%, suggesting that the water meniscus is ionized by the strong electric field to produce electrons. Since the method described here for nanopatterning is applicable for materials with significantly different physical, electronic, and optical properties, and is dependent largely on the ambient humidity level and the strength of the electric field, it is suggested that the method may be extended to a variety of other materials.

1. INTRODUCTION

Electrostatic manipulation of macromolecules [1-4] and biological objects [5] at the nanoscale is a useful and innovative approach for various aspects of nanotechnology such as ultra-dense data storage, molecular electronics, and bio-nano-electromechanical systems. In most cases, the key tool for the manipulations of molecules on surfaces is an electrically biased atomic force microscope (AFM) tip operated under ambient humidity. Humidity plays an important role in water-meniscus-generated friction at the nanoscale [6] and is also a critical factor that affects electric current density in the tip-surface junction with regards to nanoscopic feature patterning and their lateral resolution. It has also been shown that nanometer-size menisci of organic liquids may sustain chemical reactions [7], and that the properties of menisci depend on the field-induced polarization of the water layer adsorbed on the surface, the surface energy, and ambient water condensation from humid air [8]. A modeling of induced water condensation [9], and free energy analysis of the system comprising of the tip, a water bridge, and a dielectric surface suggests water polarization due to the external electric field plays an essential and affects tip dynamics [10]. Furthermore, it has been shown that the formation of a water meniscus in the proximity of an AFM tip is a major factor in electric charge transport [11] and generation of charge carriers [12] at the tip-surface junction. Experimental analysis [1-4, 11,12] of electric currents generated by a weakly biased AFM tip through various polymeric films (including polystyrene, polymethylmethacrylate, and fluorinated polybenzoxazole) of different molecular structure and molecular weights in the range 2,000-2×10^6, and also through the surface of silicon suggests the following scenario: a negatively biased AFM tip (-1 to - 40 V), either dwelling or slowly moving 0.5 – 5.0 nm above the surface, mediates an *electric breakdown* in the water meniscus due to field-induced water ionization as demonstrated on silicon surface [12]. The ionization of water produces electrons (e^-), protons (H^+) and hydroxyl radicals ($OH^•$) according to the following reaction: $H_2O \rightarrow e^- + H^+ + OH^•$ [9]. The field required to induce the latter process is of the order of 10^9 Vm^{-1}, which is a typical of the magnitude of the electric field in the proximity of a weakly biased AFM tip apex. The result of this chemical reaction is an abundance of electrons, which carry the current through the water meniscus. Other radical species generated through field-induced ionization may be consumed by recombination and related processes.

The behavior of the water meniscus between a surface and a nanoasperity under conditions of extreme electrostatic field is complicated. The objective of this study is to experimentally study and describe the influence of ambient humidity, from which the water meniscus is formed by condensation, on nanostructure formation on the surfaces of thin films of polymers and a-CdS. The choice of these materials with completely different physical, electronic, and optical properties in this study is not accidental: an understanding of how amorphous surfaces and macromolecules respond to maskless functionalization is important for photovoltaic cell design and fabrication.

2. EXPERIMENTAL SECTION

Polymer films were deposited onto conductive Au-Pd surfaces evaporated on Si (111) as follows. (1) From a 1% wt. solution of poly-(methylmethacrylate) (PMMA), molecular weight 850k diluted in toluene spin cast at 2000 rpm for 20 s, followed by 6000 rpm for another 20 s, and (2) from a 0.5% wt. solution of polystyrene, 110k molecular weight spin cast at 3000 rpm for 20 sec, also followed by 6000 rpm for another 20 sec. Each sample was cured for 20 minutes on a hot plate at a temperature 125 °C which is above the glass transition points of PMMA and PS. Part of the film on each sample was removed to allow a conductive electrode to be attached. The thickness of the films was estimated to be between 20 and 40 nm and therefore suitable for Atomic Force Microscopy-assisted Electrostatic Nanolithography (AFMEN) protocol which is typically employed for films thinner than 1 μm. AFMEN protocol [1-5] utilizes a controlled electric bias (0-50 V) through a thin dielectric film (20-300 nm) between an AFM tip a planar counter electrode beneath the film. An electric breakdown at the nanoscale deforms the dielectric film (softens polymer) directly under an AFM tip via localized Joule heating. A dielectric is polarized and electrostatically attracted to an AFM tip in very strong electric field (10^8 –10^{10} V/m) generating features. AFMEN allows rapid creation of nanostructures as small as 5-50 nm wide, and 0.5 – 100 nm high without external heating of the dielectric of AFM tip-surface junction [1, 5].

*Address correspondence to this author at the Department of Physics, The University of Akron, OH 44325, USA; Tel: (330) 972-8356; E-mail: sfl@physics.uakron.edu; sfl@uakron.edu

1573-4137/08 $55.00+.00

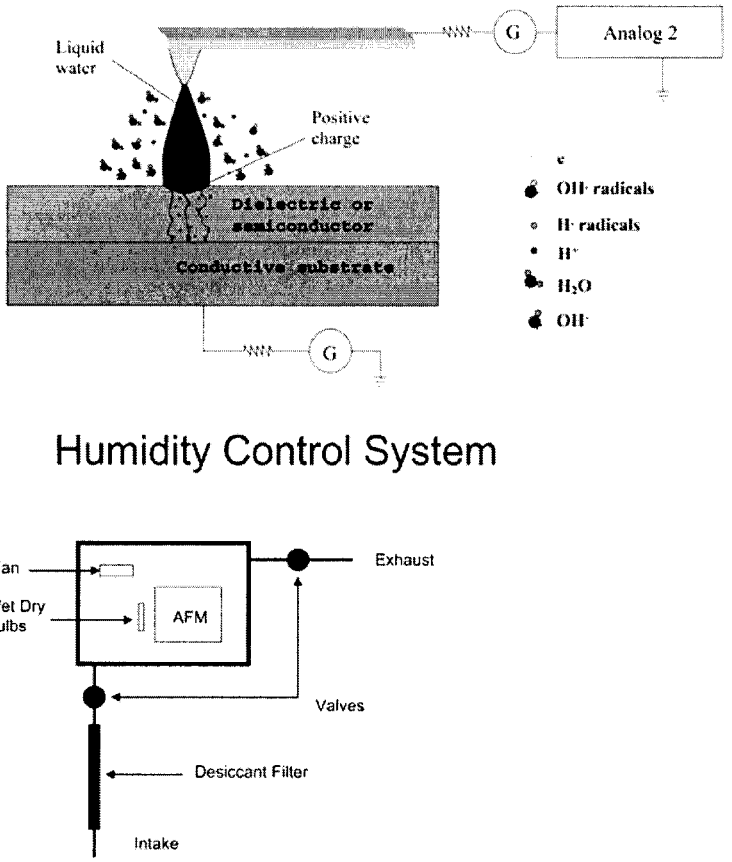

Fig. (1a). Experimental configuration of the tip/water meniscus/surface system. The system is effectively a nanoscale electrochemical cell. The water monolayer on the dielectric and other surfaces has been omitted for clarity. **(b)** The humidity is monitored by wet/dry bulbs, and controlled using a dynamic gas filtration system.

CdS films were RF sputter deposited onto commercially available 100 nm thick Au-Pd coated silicon wafer substrates. A high purity (99.999%), CdS target supplied by Kurt J. Lesker Co., was used as the source material. Sputtering was performed in an inert argon background at a pressure of ~ 50 mTorr, and films were formed at a very low deposition rate (~ 0.01 – 0.02 nm s^{-1}) to ensure they were smooth and uniform (roughness less than 2 nm) as was confirmed by subsequent AFM tapping mode imaging. Film thicknesses were determined *in situ* using a quartz crystal microbalance, and ranged from 100 – 500 nm. Full details of our sputtering method and electrical and topological characterization the CdS films can be found elsewhere [14].

A Veeco Metrology 3100 Dimensions scanning probe microscope (SPM) with a Nanoscope IV controller was used to execute standard AFMEN protocol [1]. Typically, the tip is manipulated at a height of 0.5 – 1 nm above the surface and over 1-4 μm square area, exposing the surface to 1-2 s electric pulses at randomly selected points. The specifics of the protocol can be found elsewhere [1-4]. It is essential that the AFMEN protocol sustains water meniscus formation when operating in contact mode. A positive or negative tip bias voltage was applied which varied between 0 and 50 V DC magnitude.

The input (i_{in}) and output (i_{out}) electric currents were monitored with a 5400 Keithly pico-ammeter. The input current was measured by connecting the pico-ammeter in series between the Analog 2 output of Nanoscope IV controller and the tip directly. The output current was measured using the same pico-ammeter connected in series between a conductive substrate and the ground. The currents were digitized and recorded on PC.

The humidity during the experiment was controlled by isolating the entire AFM system in a closed hood which was supplied by a filtered gas intake line. A desiccant filter and compressed air or N_2 was used to provide the gas supply. An exhaust line was incorporated to allow moist air to escape and to avoid pressure build up under the hood. The exhaust and intake ports are located inside the hood at opposite ends. An internal fan ensures that the air inside is mixed thoroughly and the humidity was monitored continuously using wet/dry thermometers and a web cam under the hood. Three different hydrometers (two digital and one based on wet/dry bulbs) were used to monitor the humidity level. The experimental arrangement yields a minimum level of humidity (10%) under the AFM hood. Once the desired humidity is reached, the intake and exhaust ports are closed using valves located outside of the unit. The internal fan is then shut off leaving a stable condition to perform experiments with AFM.

3. RESULTS AND DISCUSSION

The system in the present study is effectively an electrochemical cell comprised of the tip, a water bridge, unsaturated water vapor formed in vicinity of the tip due to electrostatic attraction of water molecules to the biased tip, and a surface film. The system is shown schematically in Fig. (**1a**). The humidity in the system is maintained and controlled by a dynamic filtered air flow method.

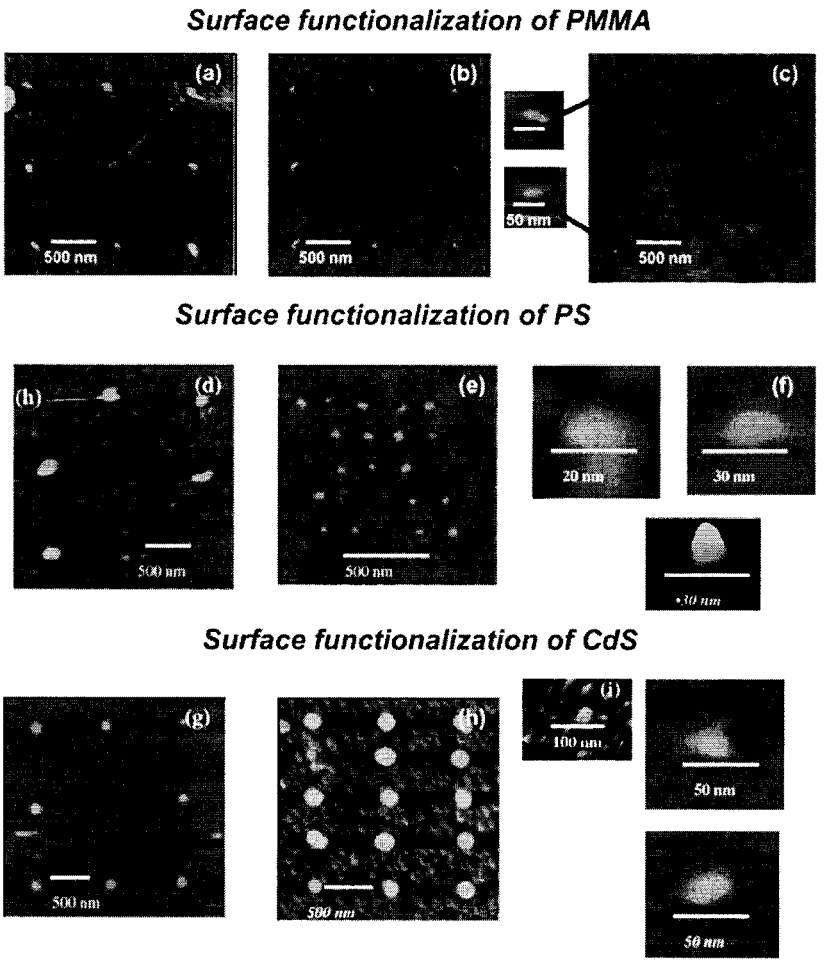

Fig. (2a). through (c). Examples of patterning in a 30 nm thick region of 850k-PMMA film using AFMEN protocol. **(a)** H_r = 43%. The output current i_{out} varies from -60 nA to 1.8 A producing dots between 50 and 70 nm wide. The height of the dots is between 2 and 4 nm **(b)** H_r=30%. The voltage varies between -10 and -14 V and i_{out} varies between -70 and 1200 nA. The width of the nanostructures is reduced to 30-40 nm and their height varies between 2 and 4 nm. **(c)** H_r=20%. The voltage varies between -10 and -14 V, and i_{out} varies between -100 and 800 nA. The width of the nanostructures is 15-25 nm. Insets: Two nanodots patterned at -10 and -12 V respectively under 20% humidity. The height of the dots is between 2 and 4 nm and the temperature is T = 24 ^{0}C.

Fig. (2d). through (f). Nanostructures patterned in the surface of 50-nm thick 110K polystyrene film using AFMEN protocol. Examples of raised structures: **(d)** H_r above 50%. Output current i_{out} exceeds input current for -15 V and reaches -15 nA. At this level of humidity the surface functionalization is not repeatable: both raised structures (the width varies from 100-200 nm) and holes are patterned in the surface. **(e)** H_r=23%. Output current i_{out} exceeds input current for -20 V and reaches -12 nA. The width of the structures varies between 30 and 50 nm. **(f)** H_r was less than 15%. Output current never exceeds input current; the width of the structures is between 14 and 17 nm, and the height is less than 2 nm; Temperature is 19 ^{0}C.

Fig. (2g). through (i). Nanostructures patterned in 50-100 nm thick CdS films using same protocol. **(g)** H_r> 50%. The electric voltage did not exceed -20 V. The height of the structures varied between 4 and 10 nm, and the width between 150 and 170 nm. **(h)** H_r = 25%. An array of dots was patterned for the tip bias -18 V. The width of the structures was between 100 and 150 nm, and the height of the structures varied between 5 and 7 nm; **(i)** H_r < 17%. The width of the patterned dots was 40-50 nm, the height of the dots was less than 5 nm; In all experiments the temperature was maintained around T = 19 ^{0}C.

Fig. (**2**) presents topographical images of the surfaces illustrating the effect of humidity on surface functionalization of three different materials: poly-(methacrylate) (PMMA), polystyrene (PS), and amorphous CdS. For all the samples, AFMEN protocol [1] was applied under variable humidity conditions (H_r varied from 10 to 60%). For PMMA samples nanostructures (raised dots) are formed on the surface and their width decreases with humidity from 50-70 nm (H_r = 43%, Fig. **2a**), to 15-25 nm (H_r = 14%, Fig. **2c**). The tip moves above the dielectric surface over a square 2×2 μm area patterning an array of 8 dots. Nanostructures are formed for negative voltages between -10 to - 15 V at each marked point (but not between the points) for an exposure time between 0.1 and 2 sec. The height of the features, however, remains essentially independent of the humidity and was determined to be between 2 and 4 nm. We have observed that in AFMEN the tip-sample separation typically varies between 0.5 and 5 nm, and this separation determines the *height* of water meniscus, and thus the feature height. A similar trend was observed in PS samples. The width of the structures patterned using the very same conditions decreases with humidity from 90 nm (H_r above 50%, Fig. **2d**) to 14 nm (H_r < 15%, Fig. **2f**). Once again, the height of the nanostructures is not affected substantially by the humidity, and was found to be in the range of 1-4 nm. Although both positive (0+30 V) and negative (0-32 V) tip bias is used, the raised structures are patterned for negative bias only. Ablation of the surface is observed for the positive tip bias above + 20 V (see inset). When AFMEN protocol was applied to CdS surfaces, it was also observed that the width of the patterned structures decreases with humidity from 170 nm (H_r above 50%, Fig. **2g**) to 40 nm (H_r<17%, Fig. **2i**).

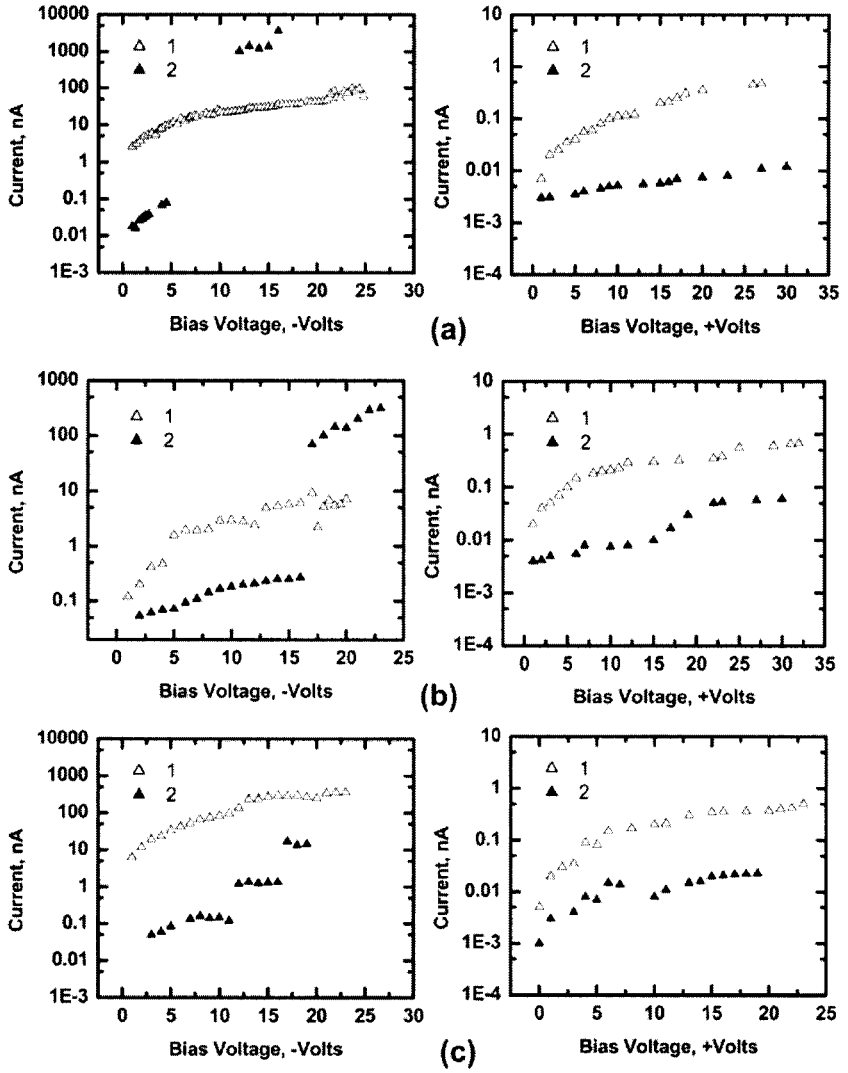

Figure 3(a) through (c). Input (open triangles), and output (closed triangles) currents versus tip bias voltage for a PMMA film. **(a)** 10-nm PMMA film at H_r = 40%.. **(b)** 30-nm PMMA film at H_r = 20%. **(c)** 30-nm PMMA film at H_r = 14%.

To analyze conductivity processes and charge transport, a substantial amount of *i*-V data were collected. Fig. (**3**) presents a comparison of *i*-V dependencies, recorded at different humidity levels, for PMMA, PS, and CdS films deposited on Au-Pd conductive substrates. The plots show the input (i_{in}) and output (i_{out}) currents. The results for PMMA are presented in Fig. (**3** (**a**)) H_r=43%, (**b**) H_r=20 (**b**), and (**c**) H_r=14% for negative and positive tip bias. We define forward bias when the AFM tip is negative and reverse bias when it is positive. For the 10-nm PMMA film at H_r = 40%, Fig. (**3**(**a**)), under negative bias the input current varies between 2.6 and 96 nA and the output current exhibits sharp increase from the pA-range up to 10^3 nA exceeding input current by at least one order of magnitude. The raised circular structures are formed in the film for an output current above 10^3 nA as shown in Fig. (**2**(a)). For positive bias the input current varies between 7 pA and 0.5 nA and the output current never exceeds 0.012 nA for the entire range of bias voltages from +1 to +30 V. For the 30-nm PMMA film at H_r = 20%, Fig. (**3**(**b**)) under negative bias the input current varies between 0.12 and 7.2 nA and the output current again changes two orders of magnitude from 200-250 pA to 70-315 nA. Raised structures are formed in the polymer surface when the output current jumps by an order of magnitude. For positive bias the input current varies between 20 pA and 0.7 nA, while the output current between 4 pA and 0.6 nA. A nearly linear *i*-V dependence for the experimental points above the electric breakdown threshold in case of negative tip bias was observed. For the 30-nm PMMA film at H_r = 14%, Fig. (**3**(c)), under negative bias the input current varies between 3 and 365 nA, while the output current changes in steps between 0.06 and 0.12 nA, 1.22 and 1.36 nA, 14.6 and 17 nA. No abrupt change of the output current observed and no evidence of nanostructures formed at this level of humidity can be provided. In summary, the pattern is different for the positive and negative bias voltages. For negative bias, an abrupt change of the output current with respect to the input current was observed, while i_{in} varied between 0.1 and 365 nA, the output current abruptly jumped from 10-100 pA to 10^3 nA at humidity levels exceeding 20% as shown in Fig. (**3**(**a**)) and (**b**). The magnitude of the bias voltage at which the output current abruptly changed several orders of magnitude varied from -5 V to -20 V. It was found that *i*-V dependencies do not show the same trend for H_r lower than 20%. Although i_{out} shows step-like behavior, its magnitude in this case never exceeds i_{in} as shown in Fig. (**3** (**c**)). In all our observations the output current has never exceeded the input current for positive bias.

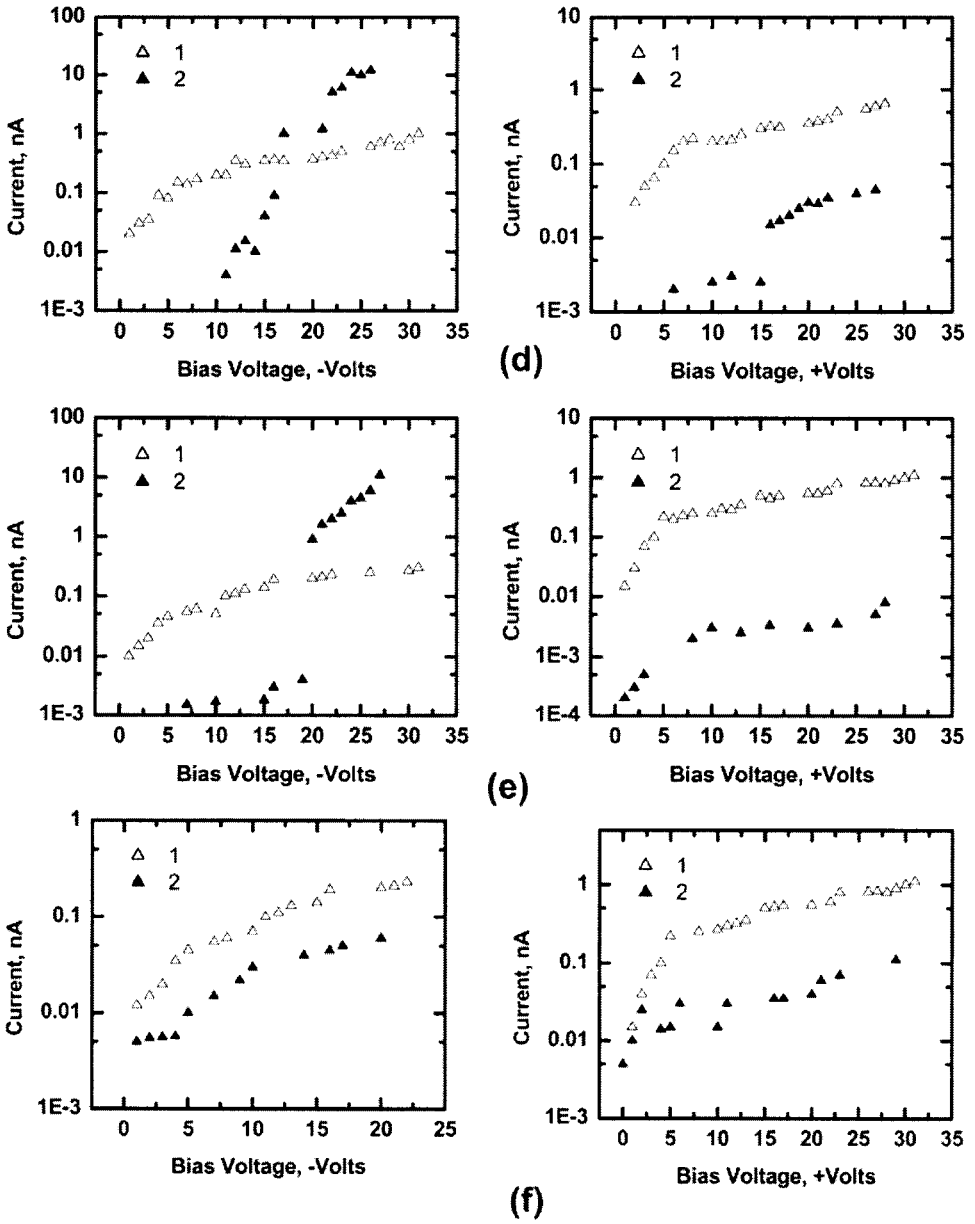

Fig. (3d). through (f). Input (open triangles), and output (closed triangles) currents versus tip bias voltage for a 30-nm PS film **(d)** H_r = 50%. **(e)** H_r = 26-30%; **(f)** H_r = 10-12%.

For the 30 nm PS film, the results are presented in Fig. (**3** (**d**)) H_r = 50% (e) H_r = 26-30% (f) H_r = 10-12% for negative and positive tip bias. At H_r = 50%, Fig. (**3**(d)) and under negative bias the input current varies between 20 pA and 1 nA, and the output current between 4 pA and 12 nA showing dramatic increase above the bias voltage -15 -18 V exceeding the input current for an order of magnitude. For positive bias, the input current varies between 30 pA and 0.7 nA and output current between 10 pA and 45 pA never exceeding the input current. Raised nanostructures formed in case of negative bias, and depressed structures formed in case of positive bias, as indicated on the inset of Fig. (**2**(**d**)). At H_r = 26-30% under negative bias, Fig. (**3**(**e**)), the input current varies between 10 pA and 0.3 nA, the output current changes between 1 pA and 11 nA exceeding input current for the bias larger than -20 V. For positive bias, the input current varies between 15 pA and 1.1 nA and output current between 1 and 8 pA. Nanostructures repeatedly formed for negative bias only. At H_r = 10-12% under negative bias, Fig. (**3**(**f**)), the input current varies between 12 pA and 250 pA and the output current between 5 pA and 60 pA. For positive bias, the input current varies between 15 pA and 1.1 nA and the output current was very low varying between 5 and 110 pA. No nanostructures were patterned for the positive tip bias. Once again, the patterns for negative and positive tip bias differ. The output current for the negative bias at humidity level above 25% jumped several orders of magnitude up to 1-2 nA (H_r = 50%) and to 1 nA (H_r = 26-30%). This trend was neither observed at low humidity nor for reverse tip bias; the nanostructures only formed under negative tip bias.

Figs. (**3** (**g**)) through 3 (**i**) are current-voltage curves obtained by positioning the AFM tip in close proximity to CdS films (0.5 – 5.0 nm) while maintaining the ambient humidity at two different

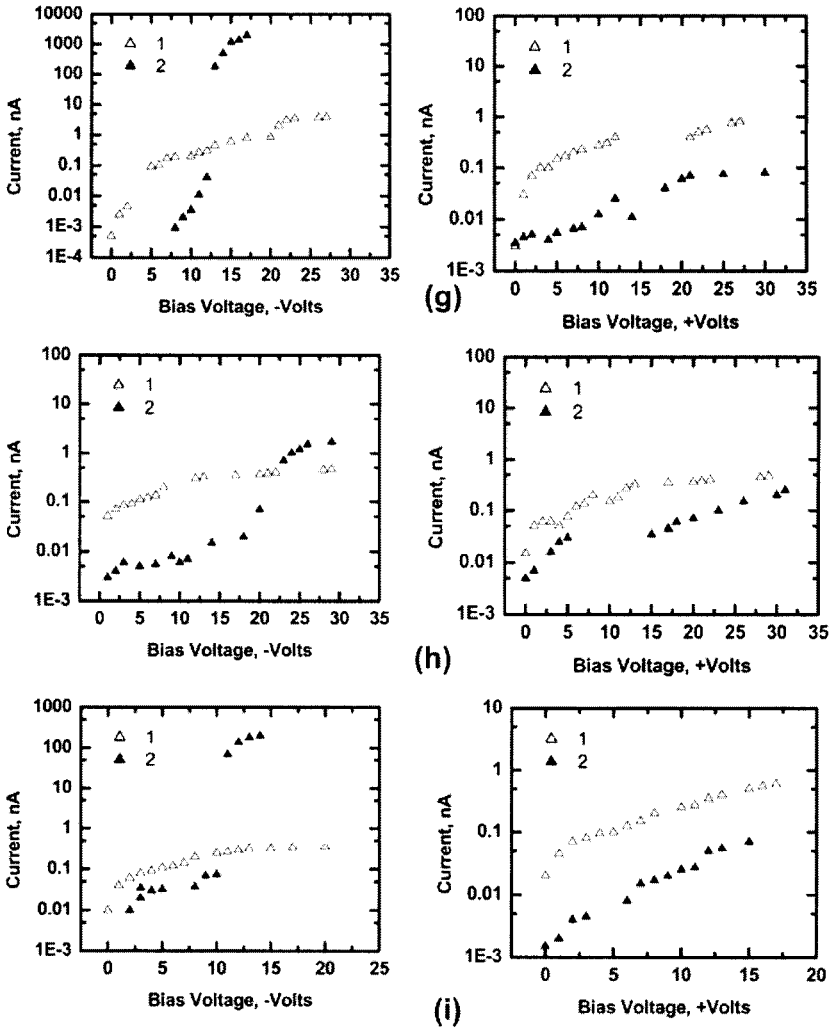

Fig. (3g). through (i). Input (open triangles), and output (closed triangles) currents versus tip bias voltage for a 100 nm CdS film. **(g)** H_r = 48-50%. **(h)** H_r = 20-24 **(i)** H_r = 10-14%.

levels. Fig. (**3** (g)) shows forward and reverse bias *i*-V plots obtained at an ambient humidity above 50%, and Fig. (**3** (**h**)) is forward, and reverse bias plots at humidity 20-24%. At H_r = 48-50% under negative bias, Fig. (**3**(g)), the input current varies between 5 pA and 4 nA, and the output current between 1 pA and 2 μA with abrupt increase from nA to μA range for the bias voltage around -12 -13 V exceeding the input current for several orders of magnitude. Fuctionalized CdS surface as shown in Fig. (**2**(**g**)). For positive bias the input current varies between 5 pA and 0.8 nA, and the output current between 3 pA and 80 pA never exceeds the input current. At H_r = 20-24%, under negative bias, Fig. (**3**(**h**)), the input current varies between 50 pA and 470 pA, the output current changes between 3 pA and 1.7nA with the increasing input current for the bias voltage around -23 to -24 V. Raised nanostructures patterned in the surface are presented in Fig. (**2**(h)). For positive bias the input current varies between 15 pA and 500 pA, and output current between 5 pA and 250 pA never exceeds the input current. At H_r = 10-14%, under negative bias, Fig. (**3**(**h**)), the input current varies between pA and pA, and the output current changes between 10 pA and 200 nA with abrupt increase of the output current for the bias voltage around -11 -22 V. For this case surface of the sample was ablated and no nanostructures were formed. Raised nanostructures patterned in the surface for the bias voltage below -10 V are presented in Fig. (**2**(**i**)). For positive bias the input current varies between 20 pA and 600 pA, and output current between 1.5 pA and 70 pA never exceeds the input current. As can be seen, for the lower humidity conditions the input and output currents correlate well under both forward and reverse bias. Both input and output currents increase by approximately 2 orders of magnitude as the bias is increased from 0 to 35 V. However, for higher humidity, the output current increases by almost 7 orders of magnitude while the input current only increases by 3 or 4 orders of magnitude as shown in (Fig. **3** (**g-i**)).

The overall similarity of the current-voltage trends for both insulating (PMMA, PS) and semiconductor (CdS) substrates suggests that the water meniscus plays a major role in supplying charge for the process. Generation of electrons in the meniscus is triggered at voltages exceeding a substrate-specific threshold, provided that the relative humidity stays above 20%. As a consequence, the measured output current increases while the input current stays limited. For polymeric films, the current inside the film is carried by electrons under the breakdown regime [1,3].

Water vapor tends to condense in tiny pores and cavities due to the combined influence of geometrical confinement and intermolecular attraction between the water molecules through hydrogen

bonding. The thresholds for the pressure and the humidity required for water condensation are especially low when the confinement length scale is comparable to the size of the molecules [15]. Nanoscale confinement of water vapor at an AFM tip - surface junction results in a distinct water meniscus in the liquid phase under ambient conditions. The size of the meniscus, as experimentally observed by Rozhok *et al.* [16] and Weeks *et al.* [17] and theoretically shown by Jang *et al.* [18] and Paramonov *et al.* [19], grows with ambient humidity. The electric field in the tip-surface junction further enhances water condensation [20], which strongly affects the surface functionalization with biased AFM tip.

Electrons in the region between a conductive AFM tip and a conductive backplane may originate from the three following sources: 1) electrons tunneling from the conductive tip, 2) water ionization [1,12], and 3) electrons generated on defects and impurities inside of the polymer film [21] .The fact that i_{out} was found to be greater than i_{in} for most cases at H_r above 20-25% suggests that factor (A) is not the major one. The electric breakdown was observed in various polymer films of different chemical structure [1-4]. This experimental fact suggests that the major factor for unusually high electric current drained through the polymeric films (1-1000 nA), and also through amorphous semiconductor (10-1000 nA) should *not* be charge generation on the defects and impurities 3). Although factors 1) and 2) may play a dominant role in other experimental situations, this study allows separation of the factor 2) by simultaneously monitoring the input and output currents.

4. SUMMARY

Experimental analysis of the electric current-voltage behavior and the surface functionalization of polymer and semiconductor surfaces, using AFMEN protocol, have been performed for various relative humidity levels. Our results, combined with the previous studies [1,3,12] suggest that electrons supplied by water ionization are responsible for the sustainable electric current in the tip-sample junction. Furthermore, the current through the films exceeds the input current through the tip by an order of magnitude for relative humidity levels H_r > 20-25%. The magnitudes of the electric currents, which were estimated based on the calculated electric field distribution in the tip-sample junction and the water self-diffusion rate, agree with the measured current levels indicating that water ionization in the meniscus is a likely factor contributing to the large output current.

For the polymer films, the nanostructure formation process is associated with mass transport (displacement) of the macromolecules in a strong electric field gradient, while for the semiconductor film (CdS) the process likely involves surface ionization and ionic transport, possibly combined with electrochemical oxidation. The similarity of the surface patterning in materials with significantly different physical and chemical properties, in this case semiconductor (CdS) and polymer (PMMA and PS) films, suggests that the observed characteristics of nanostructure formation are primarily determined by the water meniscus. The lateral size of the nanostructures fabricated at different levels of humidity increase with humidity. Interestingly, the structures patterned at relative humidity below 20% were 15-25 nm in diameter – which is smaller than the curvature of the AFM tip apex, and provides an additional means of control over patterning at the nanoscale.

ACKNOWLEDGEMENTS

This work was supported by USAF/University of Akron STW-21 Program which continues from 2002, and funded through AFOSR Grant FA 90-05-1-0471-3. S.F.L. acknowledges the Materials and Manufacturing Directorate (Nonmetallic division), Air Force Research Laboratory, WPAFB for hospitality during his Summer Faculty Fellowship 2002-2004 awarded by the National Research Council.

REFERENCES

[1] Lyuksyutov, S. F.; Vaia, R. A.; Paramonov, P. B.; Juhl, S.; Waterhouse, L.; Ralich, R. M.; Sigalov, G.; Sancaktar, E. *Nat. Mater.,* **2003**, *2*, 468.
[2] Lyuksyutov, S. F.; Vaia, R. A.; Paramonov, P. B.; Juhl, S. *Appl. Phys. Lett.,* **2003**, *83*, 4405.
[3] Lyuksyutov, S. F.; Paramonov, P. B.; Sharipov, R. A.; Sigalov, G. *Phys. Rev. B,* **2004**, *70*, 174110.
[4] Juhl, S.; Phillips, D.; Vaia, R. A.; Lyuksyutov, S. F.; Paramonov, P. B. *Appl. Phys. Lett.*, **2004**, *85*, 3836.
[5] Lyuksyutov, S. F. *Curr. Nanosci.*, **2005**, *2*, 245.
[6] Sirghi, L. *Appl. Phys. Lett.*, **2003**, *82*, 3755.
[7] Martinez, R. V.; Garcia, R. *Nano Lett.*, **2005**, 5, 1161.
[8] Gomez-Monivas, S.; Saenz, J. J.; Calleja, M.; Garcia, R. *Phys. Rev. Lett.*, **2003**, *91*, 056101.
[9] Sacha, G. M.; Verdauger, A.; Salmeron, M. *J. Phys. Chem. B.,* **2006**, *110*, 14870.
[10] Lyuksyutov, S. F.; Paramonov, P. B.; Mayevska, O. V.; Reagan, M. A.; Sancaktar, E.; Vaia, R. A.; Juhl, S. *Ulramicroscopy,* **2006**, *106*, 909.
[11] Bloess, H.; Staikov, G.; Schultze, J. W. *Electrochim. Acta,* **2001**, *47*, 335.
[12] Lyuksyutov, S. F.; Paramonov, P. B.; Dolog, I.; Ralich, R. M. *Nanotechnology,* **2003**, *14*, 716.
[13] Pinkerton, T. D.; Scovell, D. L.; Johnson, A. L.; Xia, B.; Medvedev, V.; Stuve, E. M. *Langmuir,* **1999**, *15*, 851.
[14] Dolog, I.; Mallik, R. R.; Malz, D.; Mozynski, A. *J. Appl. Phys.,* **2004**, *95*, 3075.
[15] Gelb, L. D.; Gubbins, K. E.; Radhakrishnan, R.; Sliwinska-Bartkowiak, M. *Rep. Prog. Phys.*, **1999**, *62*, 1573.
[16] Rozhok, S.; Sun, P.; Piner, R.; Lieberman, M.; Mirkin, C. A. *J. Phys. Chem. B,* **2004**, *108*, 7814.
[17] Weeks, B. L.; Vaughn, M. W.; DeYoreo, J. J. *Langmuir,* **2005**, *21*, 8096.
[18] Jang, J.; Schatz, G. C.; Ratner, M. A. *J. Chem. Phys.*, **2002**, *116*, 3875.
[19] Paramonov, P.B.; Lyuksyutov, S. F. *J. Chem. Phys.*, **2005**, *123*, 084705.
[20] Garcia, R.; Calleja, M.; Rohrer, H. *J. Appl. Phys.*, **1999**, *86*, 1898.
[21] Kroschwitz, J. I. (Ed.) *Electrical and Electronic Properties of Polymers: A State-of-the-Art Compendium.* Wiley: New York, **1988**.

Received: September 25, 2007 Revised: November 14, 2007 Accepted: November 20, 2007